

Dual Energy Inverse Mapping Technique to Estimate Calcium-to-Phosphorus Mass Ratio in Bone Quality Assessment

Panagiota I. Sotiropoulou¹, George G. Fountos², Niki D. Martini¹, Vaia N. Koukou¹, Christos M. Michail², Ioannis G. Valais², Ioannis S. Kandarakis² and George C. Nikiforidis¹

1. Department of Medical Physics, Medical School University of Patras, Patras, Greece
2. Department of Biomedical Engineering, Technological Educational Institution of Athens, Athens, Greece,
gfoun@teiath.gr

Abstract

Bone quality is a broad term encompassing factors affecting the structural and material properties of bone. X-ray dual-energy method (XDEM) provides one way to explore bone quality in terms of bone tissue material properties. In this study a XDEM is presented for the determination of Ca/P mass ratio, parameter which appears to play an important role in bone health. The low- and high-energy intensity measurements were combined, using a nonlinear mapping function, to cancel out the soft tissue structures and generate the dual energy (DE) Ca/P mass ratio value. The total entrance-skin exposure from low- and high-energy measurements was constrained so that it is similar to diagnostic-examination levels. The DE simulated data were exported using variable Ca and PO₄ thicknesses, while the tissue thickness was kept constant. The thickness of each material was fitted separately using a nonlinear least squares minimization algorithm. The functional forms of inverse functions that have been investigated are the linear, quadratic, cubic, and conic functions. The inverse-mapping functions were found to vary as analytic functions of second (conic) and third (conic) order. A nonlinear eight term rational function was selected for dual energy calibration which appeared to be capable of high fitting accuracy while requiring relative few terms.

Key words: Bone quality, dual energy X-ray, X-ray simulations, nonlinear functions, Ca/P mass ratio

Introduction

The major component and an essential ingredient of human bones and teeth is a mineral form of calcium and phosphorus called hydroxyapatite in the form of Ca₁₀(PO₄)₆(OH)₂ that gives bones and teeth their rigidity [1]. Crystal structure and chemical composition of biological apatite reflect their physiological function as a mechanical support, which is very important to the skeletal system, storage of mineral, and storage of chemical energy [2]. Substituted ions produce a change of Calcium-to-Phosphorous (Ca/P) ratio resulting in a Ca/P molar ratio which vary notable according to various factors. Many authors have determined changes in skeletal Ca/P ratio, ranging from 0.58 to 2.34 from fetus to adult [3,4,5,6,7]. The determination of calcium and phosphorus fractions in bone mineral density measurements may hold the key to better fracture risk assessment as well as more targeted therapies [8,9]. A new dual energy method, demonstrated by Fountos et al [10,11] for in vivo skeletal Ca/P mass ratio determination, meets the requirements for quality bone assessment.

Dual-energy radiography is a technique which exploits the energy

dependence of X-ray attenuation coefficients to obtain two basis-material thickness images from a pair of log-signal (negative logarithm of the relative detector signal) images [12] obtained at two different X-ray energies. For monoenergetic X-ray sources, the dual-energy equations are linear [13] and can be solved explicitly for the basis-material thicknesses. However, for the broad, polyenergetic spectra obtained from X-ray tubes, the dual-energy equations are nonlinear integral equations, which can be solved analytically, but not in closed form. Hence, various nonlinear functional forms have been used to approximate this solution [14,15]. In either case, the chosen functional form is fitted to calibration data, obtained by imaging a calibration phantom [16] and the fitted functions are then used to decompose a pair of dual-energy log-signal images into the corresponding pair of basis-material thickness images. The accuracy of the decomposed images depends primarily on how well the calibration data are fitted by the fitting function. Any systematic error in the low- or high-energy image will also degrade the accuracy of the decomposed images. The precision of dual-energy radiography can be predicted theoretically from the low- and high-energy images and the fitting function.

Although the theory of X-ray dual energy method (XDEM) for Ca/P ratio determination is well developed [10,11] some technical obstacles remain which must be overcome before this method is used in clinical practice. The algorithm for Ca/P ratio has been described considering the X-ray energy spectrum as a monochromatic photon beam with energy corresponding about to the mean energy of the spectrum. The limitations of this approximation are that (i) the energy spectra must have narrow spectral width which demands the use of heavy filtering, increasing this way the tube load, and (ii) when broad spectra with not enough energy separability are used, the equation system leads to linear dependency. Most clinical radiation systems do not provide monoenergetic X-rays; therefore, the relationship between two thicknesses and the low- and high-energy intensities is generally nonlinear. Such systems therefore require calibration. The ideal algorithm should be computationally fast, accurate and capable of extrapolation beyond the calibration region. Furthermore, the calibration procedure for this algorithm should be easily implemented and require a minimal amount of calibration data.

In this study, an optimization of dual energy method is presented [11], determining the Calcium-to-Phosphorous (Ca/P) mass ratio in the proximal phalanx of the middle finger. The method assumes that there is a three-component system: Ca, PO₄ and water. The DE simulated data were exported using variable Ca and PO₄ thicknesses, while the tissue thickness was kept constant. The thickness of each material was fitted separately using a nonlinear least squares minimization algorithm. The functional forms of inverse functions that have been investigated are the linear, quadratic, cubic, and conic functions. The low- and high-energy intensity measurements were combined, using a nonlinear mapping function, to cancel out the soft tissue structures and generate the dual energy (DE) Ca/P mass ratio value.

Materials and Methods

1. Theory

The theory, upon which the in vivo determination of Ca/P ratio in the finger was based, is similar to that described by Fountos et al [10]. The Ca/P mass ratio is obtained assuming that there is a three-component system: Ca, PO₄ and water. An analytical model, considering discrete energy bins, can be applied and the transmitted fluence incident on the detector can be expressed as follows:

$$I_{w(E_j)} = \sum_{E_j, \min}^{E_j, \max} I_o(E_j) * e^{-M_{(w,E_j)} * d_w * t}; \quad j = \ell, h, \quad (1)$$

$$I_{b(E_j)} = \sum_{E_j, \min}^{E_j, \max} I_o(E_j) * e^{-M_{(Ca,E_j)} * d_{Ca} * t_{Ca} - M_{(PO_4,E_j)} * d_{PO_4} * t_{PO_4} - M_{(w,E_j)} * d_w * t_w}; j = \ell, h \quad (2)$$

where E_ℓ and E_h corresponds to low energy (LE) and high energy (HE), $I_o(E_i)$ is the unattenuated beam, $I_w(E_i)$ is the photon beam attenuated by the water bath only, $I_b(E_i)$ is the photon intensity with the finger immersed in water, and M_{Ca} , M_{PO_4} , M_w , d_{Ca} , d_{PO_4} , d_w are the energy dependent mass attenuation coefficients and densities of Ca, PO_4 , and water, respectively.

The log-intensity value, Y_j , given by:

$$Y_j = \ln \frac{I_w(E_j)}{I_b(E_j)}; \quad j = \ell, h, \quad (3)$$

The low- and high-energy log-intensity values are made independently by using X-ray beams of different spectra. The goal of the presented dual-energy Ca/P determination is to invert the obtained log-intensity functions, $Y_j(t_{Ca}, t_{PO_4})$, into Ca thickness, $t_{Ca}(Y_\ell, Y_h)$ and PO_4 thickness, $t_{PO_4}(Y_\ell, Y_h)$. The inverse functions are nonlinear due to polyenergetic nature of diagnostic spectra. The functional forms of inverse functions that have been investigated [14,15,17] for each thickness are:

$$t_i = a_{1i} + a_{2i}Y_\ell + a_{3i}Y_h; \quad i = Ca, PO_4, \quad (4)$$

$$t_i = a_{1i} + a_{2i}Y_\ell + a_{3i}Y_h + a_{4i}Y_\ell^2 + a_{5i}Y_h^2 + a_{6i}Y_\ell Y_h; \quad i = Ca, PO_4, \quad (5)$$

$$t_i = a_{1i} + a_{2i}Y_\ell + a_{3i}Y_h + a_{4i}Y_\ell^2 + a_{5i}Y_h^2 + a_{6i}Y_\ell Y_h + a_{7i}Y_\ell^3 + a_{8i}Y_h^3; \quad i = Ca, PO_4, \quad (6)$$

and

$$t_i = (a_{1i} + a_{2i}Y_\ell + a_{3i}Y_h + a_{4i}Y_\ell^2 + a_{5i}Y_h^2 + a_{6i}Y_\ell Y_h) / (1 + a_{7i}Y_\ell + a_{8i}Y_h); \quad i = Ca, PO_4, \quad (7)$$

which correspond to linear, quadratic, cubic, and conic functions, respectively.

2. Simulated X-ray beams

Unfiltered spectra were obtained from Boone et al. [18] for a Tungsten (W) anode. The low-energy spectrum used was at 40 kVp with 400 μ m Cadmium added filtration and the high-energy spectrum was at 80 kVp with 600 μ m Holmium added filtration, both obtained with 400mAs. This filtering was performed by dividing the X-ray spectra into 1-keV wide energy bins and attenuating each energy bin by the appropriate attenuation coefficient [19]. Figure 1 show the spectra used in simulation. The total irradiated thickness was kept constant at 2.8cm.

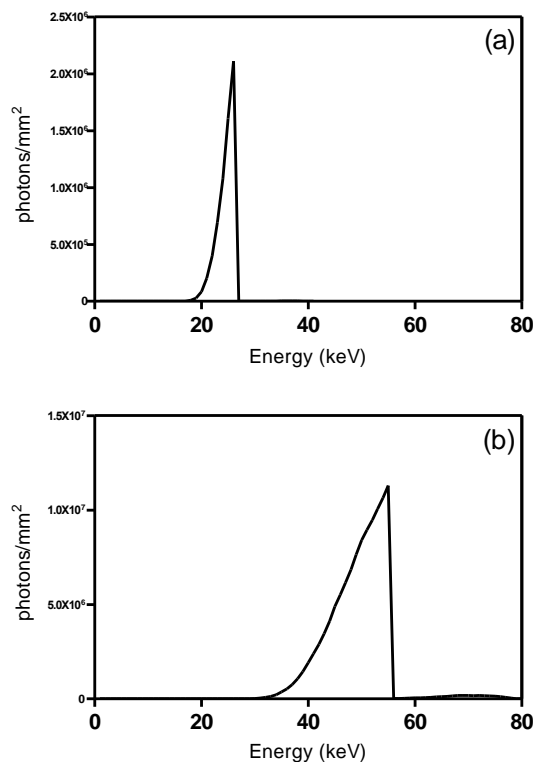


Figure 1. Spectra used in the simulations. (a) Low-energy spectrum: at 40 kVp with 400 μ m Cadmium added filtration. (b) High-energy spectrum: at 80 kVp with 600 μ m Holmium added filtration.

3. Details of simulation

The simulated calibration data were acquired at both energies for various combinations of Ca and PO₄ thicknesses. These data were obtained from seven thicknesses of each component, 0.1260-0.1488cm for Ca thickness and 0.0210-0.0400cm for PO₄ thickness. In Table 1 are shown the step thicknesses (x,y) of Ca, PO₄ used to generate detector calibration data. These thickness values correspond to published [3,4] molar Ca/P ratio from 1 to 2.5. The thicknesses combined together resulting in 49 calibration points when the total thickness maintained constant. The reference intensity level (I_0) was determined through 2.8-cm-thick water material.

Table 1. Ca and PO₄ calibration step thicknesses (in cm) used to generate simulated detector calibration data.

step	1	2	3	4	5	6	7
Ca	0.1260	0.1298	0.1336	0.1374	0.1412	0.1450	0.1488
PO ₄	0.0210	0.0248	0.0286	0.0324	0.0324	0.0362	0.0400

The accuracy determined of the statistics of the residuals was computed as the difference between the true values and the values returned by the fits in each case. The best fit was examined by the sum of squares due to error (SSE), the root mean squared error (RMSE) and the maximum absolute error (δ_{\max}) values. The SSE statistic is the least-squares error of the fit and measures the total deviation of the response values from their fitting. The RMSE is an estimation of the standard deviation of the random component in the data. A value close to zero for both SSE and RMSE indicates that the model has a smaller random error component, and that

the fitting will be more useful for prediction. Additionally, a small δ_{\max} value relative to the fitted values evaluates the fitting between the four models.

Results and Discussion

Log-intensity calculations

The calculated low- and high-energy log-intensity values are listed in Table 2 and plotted in Figure 2. The accuracy of the values presented in Table 2 could never be measured in practice but it is used to distinguish the differences in higher order functions (conic and cubic). In fact, calculations were made with even greater accuracy in the order of sixteen terms. The range of the log-intensity values are 0.2810 to 0.4254 and 0.1323 to 0.1922 for the low- and high-energy beams respectively. The maximum log-intensity values can be succeeded in higher thicknesses, where the attenuation is increased. In the low energy beam the log-intensity values vary less than in high energy beam due to greater attenuation of the photons in low energies.

Table 2. The (upper) low- and (bold) high-energy log-intensity values used in the calibration of the inverse-mapping functions.

t_{Ca}/t_{PO4}	1	2	3	4	5	6	7
1	0.2810 0.1323	0.2850 0.1344	0.2890 0.1365	0.2930 0.1386	0.2971 0.1408	0.3011 0.1429	0.3051 0.1450
2	0.3011 0.1402	0.3051 0.1423	0.3091 0.1444	0.3131 0.1466	0.3171 0.1487	0.3211 0.1507	0.3251 0.1528
3	0.3212 0.1481	0.3252 0.1502	0.3292 0.1523	0.3332 0.1544	0.3372 0.1565	0.3412 0.1586	0.3452 0.1607
4	0.3413 0.1506	0.3453 0.1581	0.3493 0.1602	0.3533 0.1623	0.3573 0.1644	0.3613 0.1665	0.3653 0.1686
5	0.3613 0.1639	0.3653 0.1660	0.3693 0.1681	0.3733 0.1702	0.3773 0.1723	0.3813 0.1744	0.3853 0.1765
6	0.3814 0.1717	0.3854 0.1738	0.3894 0.1760	0.3934 0.1780	0.3974 0.1801	0.4014 0.1822	0.4054 0.1844
7	0.4014 0.1796	0.4054 0.1817	0.4094 0.1838	0.4134 0.1859	0.4174 0.1880	0.4214 0.1901	0.4254 0.1922

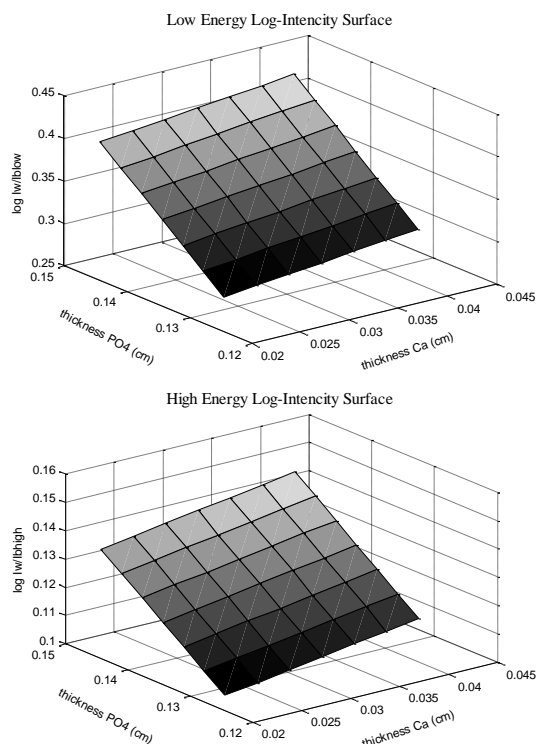


Figure 2. The calibration (top) low-energy and (bottom) high-energy log-intensity values, as a function of the Ca and PO₄ thickness, used to compute the various inverse-mapping functions.

Table 3. The root mean square error (RMSE) values, the sum of squares due to error (SSE) values and the minimum (min) and maximum (max) error values from the fit to Ca thickness and PO₄ thickness used to evaluate the accuracy of the various inverse functions.

Model function	Ca thickness				PO ₄ thickness					
	Linear	Quadratic	Cubic	Conic	Linear	Quadratic	Cubic	Conic		
RMS E	2.287E-06	5.878E-09	2.432E-11	6.916E-06	1.690E-06	1.598E-08	7.830E-11	1.578E-09		
SSE			2.407E-10	1.485E-15	2.306E-20	1.961E-09	1.314E-10	1.098E-14	2.391E-19	1.021E-16
min			-2.471E-06	-1.185E-08	-4.646E-11	-1.133E-05	-3.398E-06	-3.248E-08	-1.301E-10	-4.300E-09
max			4.739E-06	1.195E-08	4.046E-11	1.558E-05	1.840E-06	3.219E-08	1.496E-10	2.034E-09

Fitting accuracy of the polynomials

The thickness of each material was fitted separately. The coefficients (a_i) of the inverse mapping functions were statistically fitted using a nonlinear least-squares

analysis of obtained calibration data. The RMS errors for each of the inverse function are tabulated in Table 3.

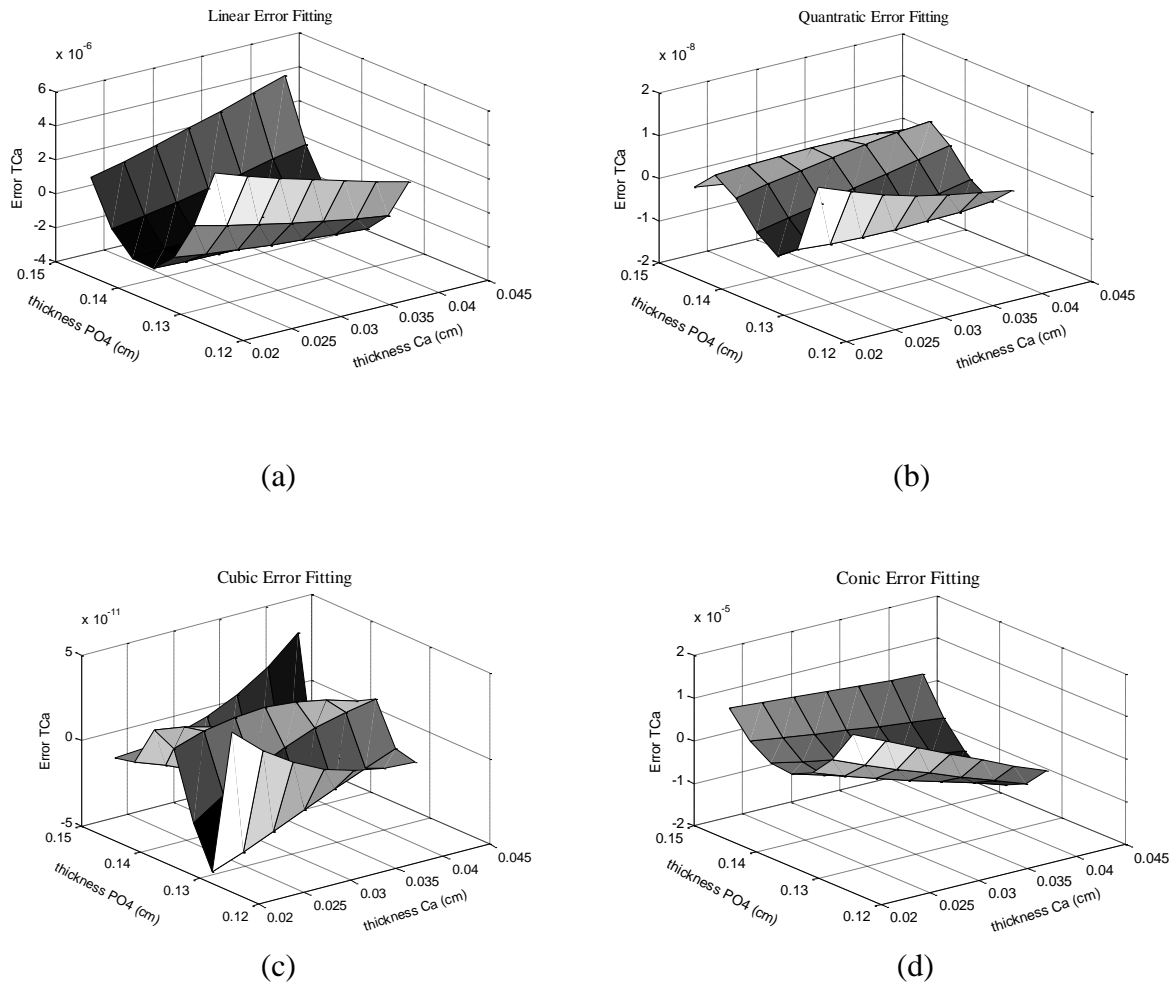
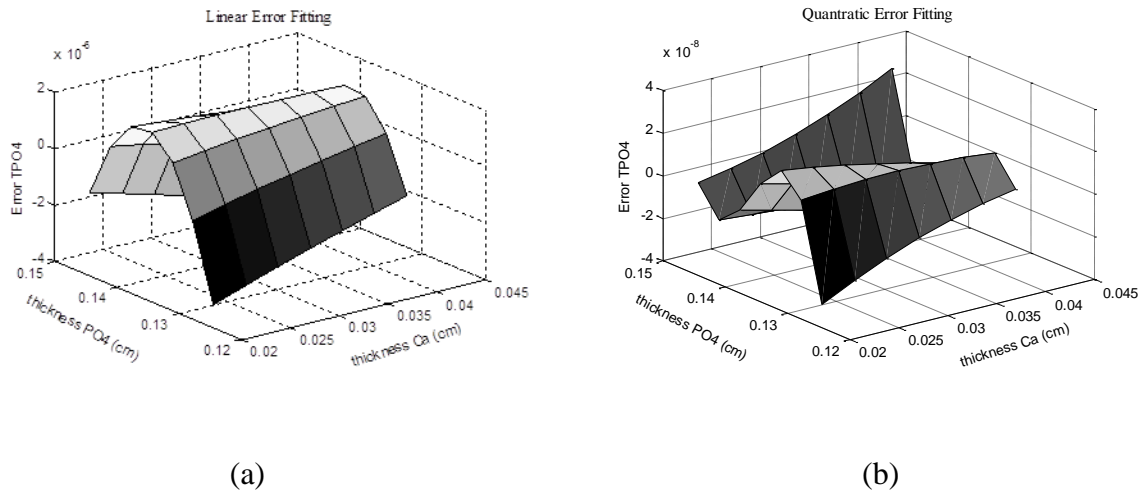


Figure 3. The residuals from the fit to Ca thickness as a function of the Ca thickness and PO₄ thickness for the (a) linear, (b) quadratic, (c) cubic, and (d) conic inverse-mapping functions.



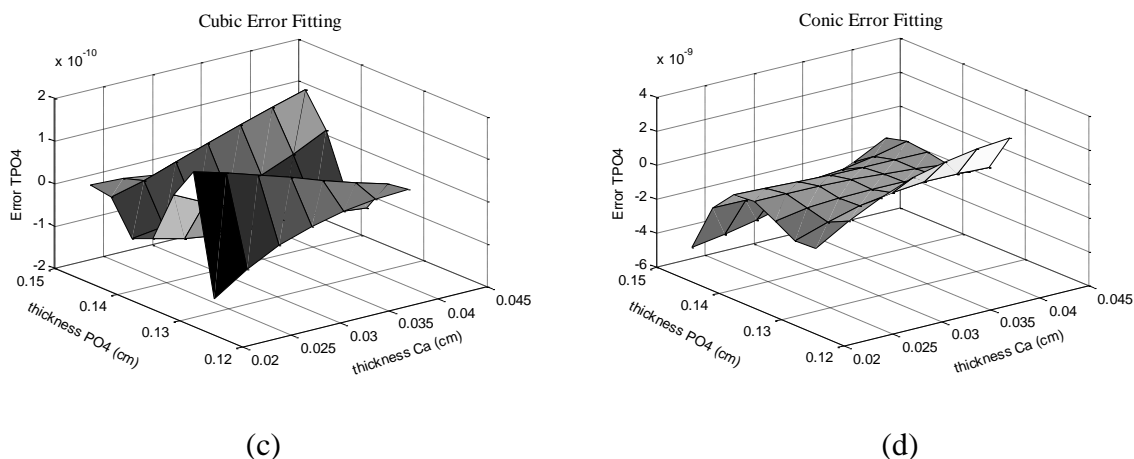


Figure 4. The residuals from the fit to PO₄ thickness as a function of the PO₄ thickness and Ca thickness for the (a) linear, (b) quadratic, (c) cubic, and (d) conic inverse-mapping functions.

The RMSE of the linear function indicate that poorly modeled the thicknesses in both cases. In the case of Ca thickness, the conic function also fails to model the thickness due to large RMSE and SSE values. The quadratic function has a better accuracy with RMSE similar for both thicknesses, but is somewhat poorer than the accuracy that could be achieved by using the cubic function. In the case of PO₄ thickness, the conic function has low RMSE and SSE values but still remains with higher values than cubic function.

Similar behaviors to RMSE have all the SSE values. The lowest SSE value is associated with the cubic function, suggesting that it might be the best fitting. The statistics reveal a substantial difference between the four equations indicating that both thicknesses modeled better by the cubic function. In cubic polynomial fit, also, the lowest maximum absolute error was achieved.

A nonlinear cubic function for each thickness was selected for dual energy calibration. These functions appeared to be capable of high fitting accuracy while requiring relatively few terms.

Conclusion

Dual-energy Ca/P determination method can be used to cancel out the water-like tissue structures and to estimate the Ca/P mass ratio in several body parts. Since there are several ways to distinguish the total thickness in a specific body part (e.g. immerse in water bath, length counter laser), the algorithm used in this study could be easily implemented, computationally fast, accurately and capable of extrapolation beyond the calibration region.

The use of various inverse mapping functions was investigated, in order to produce Ca/P accurate measures from separately acquired low and high energy images, using a photon counting detector. For the cubic inverse mapping functions, excellent correlations existed between the calculated and the true thickness. Our studies can be used as a basis for future studies on Ca/P mass ratio determination using X-ray photon counting detector.

Acknowledgement

This research has been co-funded by the European Union (European Social Fund) and Greek national resources under the framework of the “Archimedes III: Funding of Research Groups in TEI of Athens” project of the “Education & Lifelong Learning” Operational Programme.

References

1. Kay M., Young R., Posner A. “The crystal structure of hydroxyapatite”, *Nature*, 204, 1050-1052, 1964.
2. LeGeros R., Balmain R., Bonel G. “Structure and composition of mineral phase of periosteal bone”, *Journal of Chemical Research*, 77, 2313-2317, 1986.
3. Dickerson J. “Changes in the composition of the human femur during growth”, *Biochemical Journal*, 82, 56-61, 1962.
4. Woodart H. “The elementary composition of human cortical bone”, *Health Physics*, 8, 513-517, 1962.
5. Woodart H. “The composition of human cortical bone”, *Clinical Orthopaedics and Related Research*, 37, 187-193, 1964.
6. Quelch L., Melick R., Bingham P., Mercuri S. “Chemical composition of human bone”, *Archives of Oral Biology*, 8, 665-674, 1983.
7. Wopenka B., Pasteris J. “A mineralogical perspective on the apatite in bone”, *Materials Science and Engineering*, 25, 131-143, 2005.
8. Zoehrer R., Perilli E., Kuliwaba J., Shapter J., Fazzalari NL., Voelcker N. “Human Bone Material Characterization: Integrated Imaging Surface Investigation Of Male Fragility Fractures”, *Osteoporosis International*, 23, 1297-1309, 2012.
9. Tzaphlidou M., Speller R., Royle G., Griffiths J., Olivo A., Pani S., Longo R. “High resolution Ca/P maps of bone architecture in 3D synchrotron radiation microtomographic images”, *Applied Radiation and Isotopes*, 62, 569-575, 2005.
10. Fountos G., Yasumura S., Glaros D. “The skeletal calcium/phosphorus ratio: a new in vivo method of determination”, *Medical Physics*, 24, 1303-1310, 1997.
11. Fountos G., Tzaphlidou M., Kounadi E., Glaros D. “In vivo measurement of radius calcium/phosphorus ratio by X-ray absorptiometry”, *Applied Radiation and Isotopes*, 51, 273-278, 1999.
12. Alvarez R., Macovski A. “Energy selective reconstructions in X-ray computerized tomography”, *Physics in Medicine and Biology*, 21, 733-744, 1976.
13. Lemacks M., Kappadath S., Shaw C., Liu X., Whitman G. “A dual-energy subtraction technique for microcalcification imaging in digital mammography-a signal-to-noise analysis”, *Medical Physics*, 29, 1739-51, 2002.
14. Cardinal H., Fenster A. “An accurate method for direct dual-energy calibration and decomposition”, *Medical Physics*, 17, 327-341, 1990.
15. Cardinal H., Fenster A. “Analytic approximation of the log-signal and log-variance functions of X-ray imaging systems, with application to dual-energy imaging”, *Medical Physics*, 18, 867-879, 1991.

16. Lehmann L., Alvarez R., Macovski A. and Brody W, "Generalized image combinations in dual kVp digital radiography", *Medical Physics*, 8, 659-667, 1981.
17. Kappadath S., Shaw C. "Dual-energy digital mammography: Calibration and inverse-mapping techniques to estimate calcification thickness and glandular-tissue ratio", *Medical Physics*, 30, 1110-1117, 2003.
18. Boone J., Fewell T., Jennings R. "Molybdenum, rhodium, and tungsten anode spectral models using interpolating polynomials with application to mammography", *Medical Physics*, 24, 1863-74, 1997.
19. Hubbel J., Seltzer M. "Tables of X-ray mass attenuation coefficients and mass energy-absorption coefficients 1 keV to 20MeV for elements Z=1 to 92 and 48 additional substances of dosimetric interest", *National Institute of Standards and Technology*, NISTIR 5632,1995; also available at <http://physics.nist.gov/PhysRefData/XrayMassCoef/cover.html>.